High-Latitude Contribution to Global Variability of Air–Sea Sensible Heat Flux

XIANGZHOU SONG

Physical Oceanography Laboratory, Ocean University of China, Qingdao, China, and Department of Physical Oceanography, Woods Hole Oceanographic Institution, Woods Hole, Massachusetts

LISAN YU

Department of Physical Oceanography, Woods Hole Oceanographic Institution, Woods Hole, Massachusetts

(Manuscript received 9 January 2011, in final form 2 December 2011)

ABSTRACT

The study examined global variability of air–sea sensible heat flux (SHF) from 1980 to 2009 and the large-scale atmospheric and ocean circulations that gave rise to this variability. The contribution of high-latitude wintertime SHF was identified, and the relative importance of the effect of the sea–air temperature difference versus the effect of wind on decadal SHF variability was analyzed using an empirical orthogonal function (EOF) approach. The study showed that global SHF anomalies are strongly modulated by SHF at high latitudes (poleward of 45°) during winter seasons. Decadal variability of global wintertime SHF can be reasonably represented by the sum of two leading EOF modes, namely, the boreal wintertime SHF in the northern oceans and the austral wintertime SHF in the southern oceans. The study also showed that global wintertime SHF is modulated by the prominent modes of the large-scale atmospheric circulation at high latitudes. The increase of global SHF in the 1990s is attributable to the strengthening of the Southern Hemisphere annular mode index, while the decrease of global SHF after 2000 is due primarily to the downward trend of the Arctic Oscillation index. This study identified the important effects of wind direction and speed on SHF variability. Changes in winds modify the sea–air temperature gradient by advecting cold and dry air from continents and by imposing changes in wind-driven oceanic processes that affect sea surface temperature (SST). The pattern of air temperature anomalies dominates over the pattern of SST anomalies and dictates the pattern of decadal SHF variability.

1. Introduction

Air–sea sensible heat flux (SHF) is the amount of turbulent heat convection induced by the temperature difference between the ocean and the air above. When the sea surface is warmer than the near-surface air, heat is transferred from the ocean to the atmosphere as a positive SHF. Since direct measurements of SHF are limited over the global oceans, SHF is commonly estimated from the bulk aerodynamic formula that parameterizes turbulent heat process using air–sea observables (e.g., Liu et al. 1979):

$$Q_{\mathrm{SHF}} = \rho c_p c_h W(T_s - T_a), \tag{1}$$

where ρ is the air density; c_p is the specific heat capacity of air at constant pressure; c_h is turbulent exchange coefficient for SHF, which is a function of wind speed, height, and atmospheric stability; W is wind speed; and T_s and T_a are the SST and surface air temperature (SAT), respectively. It can be seen that both the wind speed and the sea–air temperature difference ΔT contributes to SHF. The effect of the temperature difference on SHF is usually referred to as the thermal effect and the effect of wind speed as the wind effect.

SHF is an energy flux that is directly related to a change in temperature. It is different from latent heat flux (LHF), which is an energy flux associated with the evaporation of water vapor from the ocean surface. In the tropical oceans where the SAT is close to SST, SHF is about one order smaller than LHF. Because of this, LHF is the predominant term in balancing the incoming solar radiation in the tropical oceans; and the contribution of SHF to the

Corresponding author address: Xiangzhou Song, Physical Oceanography Laboratory, Ocean University of China, Qingdao, 266100, China.
E-mail: oucsxz@ouc.edu.cn

DOI: 10.1175/JCLI-D-11-00028.1

tropical surface energy balance is small (Nigam and Chao 1996; Carton and Zhou 1997; Foltz and McPhaden 2005; Foltz et al. 2010). However, SHF is important at higher latitudes, particularly during the hemispheric winter season when the sea–air temperature differences are large and winds are strong. Many studies have documented that the magnitude of SHF variability is comparable to or even larger than that of LHF variability during the winter cold-air outbreak events (Grossman and Betts 1990; Xue et al. 1995; Renfrew and Moore 1999; Pagowski and Moore 2001; Renfrew et al. 2002; Yu and Weller 2009). For instance, the aircraft-based observations show that SHF can reach as high as 500 W m^{-2} while LHF is only about 100 W m^{-2} during an extreme cold-air outbreak in the Labrador Sea (Renfrew and Moore 1999). Since the incoming shortwave radiation is weak in the winter season, LHF plus SHF contributes predominantly to the change of net sea surface heat flux and drive the change of near-surface temperatures and convective mixing. Cayan (1992a) discussed the connection of LHF and SHF to the atmospheric circulation modes in the North Pacific and North Atlantic, and showed that the LHF + SHF anomalies force the local SST anomalies. The importance of LHF plus SHF in causing deep convection in the northern North Atlantic was best demonstrated in a recent study by Våge et al. (2009). An unusual deep convective overturning event in the Labrador and Irminger seas occurred in the winter of 2007/08, with a mixing of the water column to the depth of 1500 m, which had not been observed since the mid-1990s. Våge et al. (2009) found that, though the North Atlantic Oscillation (NAO) index was lower than in previous winters, the rapid, intensive sea surface cooling and subsequently deep mixing were triggered by very large latent and sensible heat loss at the sea surface resulting from unusually strong and cold westerly winds.

Several studies (e.g., Yu 2007; Yu and Weller 2007; Wentz et al. 2007) have documented the increase of LHF during the past decades, particularly from the 1980s through the 1990s when global warming was most pronounced. The enhancement of LHF with rising temperature is shown to be consistent with the theoretical projection based on the Clausius–Clapeyron equation (Boer 1993; Allen and Ingram 2002; Held and Soden 2006). However, the change of SHF in a warm climate has been less studied, although it is known that SHF is indispensible in global redistribution of radiation imbalances between incoming and outgoing components (Kiehl and Trenberth 1997; Bala et al. 2008; Trenberth et al. 2009). The global flux analysis from the Objectively Analyzed Air–Sea Fluxes (OAFlux) project (Yu et al. 2008) suggests that the decadal variability of SHF is distinctly different from that of LHF during the past

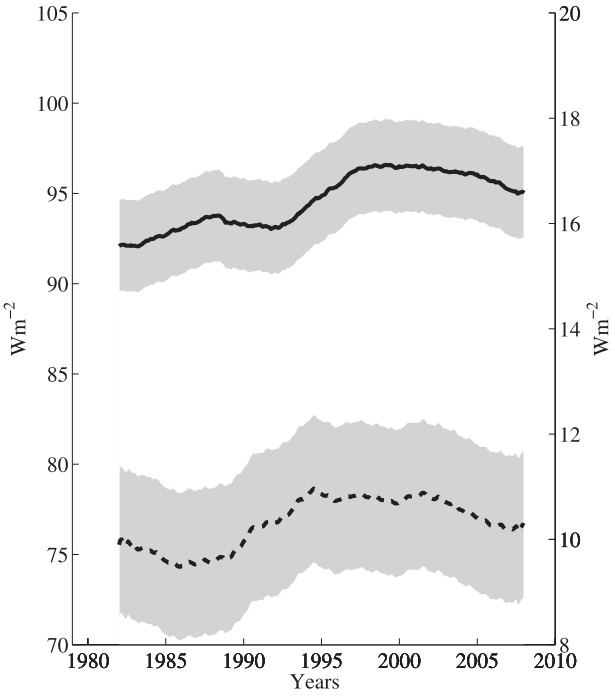

FIG. 1. Monthly time series of global averaged LHF (solid line, W m^{-2}; left axis) and SHF (dashed line, W m^{-2}; right axis). The shaded areas denote the error bars of the fluxes at the 95% confidence level. A 5-yr running mean is applied to the monthly data. The beginning and end 30 months are not plotted.

decades (Yu and Weller 2007, 2009). As shown in Fig. 1, the global monthly mean time series of SHF (dashed lower curve) from 1980 to the present is characterized by three periods: a slight downward tendency at the beginning of the time series, an upward trend from the mid-1980s to the mid-1990s, and a downward tendency from 2000 to the present. At the same time, the time series of LHF (solid upper curve) is characterized by a predominant upward tendency before 2000, followed by a slight downward tendency thereafter. There were some years that SHF and LHF both increased (such as in the early 1990s) or both reduced (such as since 2000), but the overall long-term tendency of the two time series differs. Yu (2007) reported that there is a strengthening of global wind speed in the satellite era from 1987 to the present, and that the stronger wind speed plays an equally important role as the sea–air humidity contrast in causing LHF to increase during the 1980s and 1990s. The magnitude of SHF also depends on wind speed [see Eq. (1)]. Similar to its role in the evaporation process, wind advects the heat away from the source and helps to reestablish the sea–air thermal gradient and facilitates a faster rate of turbulent conduction. Hence, two questions arise as to the role wind has played in decadal variability of SHF, and the relative importance of wind and thermal effects in giving rise to the

changing characteristics of the SHF time series. These questions will be addressed in this study.

Large SHF variability occurs mostly at high latitudes. Thus, the primary focus of the present study is on high-latitude SHF variability and its contribution to global changes. The period from 1980 and onward is chosen because this is the period when satellite observations are available and global flux estimates are better computed. The primary flux dataset used in this study is taken from the OAFlux project (Yu et al. 2008). Currently there exist several other global SHF products, such as the National Oceanography Centre Southampton flux dataset version 2 (NOCS2; Berry and Kent 2009, 2011), the Hamburg Ocean Atmosphere Parameters and Fluxes from Satellite Data version 3 (HOAPS3; Andersson et al. 2007), the Japanese ocean flux datasets with use of remote sensing observations (J-OFURO; Kubota et al. 2002), and also atmospheric reanalyzed flux products. Differences among various products have been examined by a number of intercomparison studies (e.g., Gleckler and Weare 1997; Kubota et al. 2003; Liu et al. 2010; Smith et al. 2011). A recent intercomparison by Smith et al. (2011) showed that the global comparisons of the monthly means from nine heat flux products reveal similar patterns, but with different magnitudes. This study intends to understand the cause of decadal change of SHF and its connection to the large-scale atmospheric and oceanic circulations. The understanding gained from such a study would help to better understand the large differences between various products. For this reason, only one global flux analysis is used in the present analysis.

The paper is organized as follows. Section 2 provides a brief description of datasets and methods used in the analysis. Section 3 presents the analysis of global and regional SHF anomalies and the thermal and wind effects on the generation of SHF anomalies. Section 4 shows the modes of the interaction between SHF and large-scale atmospheric and ocean circulations. Summary and conclusions are given in section 5.

2. Mean and decadal variability of SHF

a. Data

SHF, and related surface meteorological variables in this study, is developed from an objective synthesis of satellite retrievals [e.g., Advanced Microwave Scanning Radiometer for Earth Observing System (EOS) (AMSR-E), Advanced Very High Resolution Radiometer (AVHRR), Special Sensor Microwave Imager (SSM/I), and Quick Scatterometer (QuikSCAT)] and the surface meteorology from reanalysis/forecast models [e.g., National Centers for Environment Prediction (NCEP), the 40-yr European Centre for Medium-range Weather Forecasting (ECMWF) Re-Analysis (ERA-40), and ERA-Interim (Yu and Weller 2007; Yu et al. 2008)]. The objective analysis is used to obtain optimal estimates of flux-related surface meteorology, and the global fluxes are computed using the state-of-the-art bulk flux parameterizations (Fairall et al. 2003). For detailed descriptions of the methodology and strategy of the OAFlux project and validations of the products, readers are referred to the documents by Yu and Weller (2007) and Yu et al. (2008). The SHF estimates are accurate within 1 W m^{-2} (or 10%) when compared with in situ flux buoy measurements acquired over 120 buoy locations. OAFlux products include LHF, SHF, and also the flux-related surface meteorological variables such as wind speed, air/sea temperatures, and specific humidities, all of which are constructed on daily and 1° grid resolution. This study focused on the decadal variability and used monthly time series.

To investigate the interaction between SHF and large-scale atmospheric and ocean circulations, global fields of sea level pressure (SLP) and near-surface wind are needed. For this purpose, monthly SLP, zonal U and meridional V wind components from NCEP–Department of Energy (DOE) reanalysis II (hereafter NCEP2; Kanamitsu et al. 2002) are used. NCEP2 surface products are gridded on 1.875° resolution and are available from 1979 to the present.

b. Mean SHF

Figure 2 shows the global 30-yr mean SHF patterns in two seasons, the boreal winter season from December to February (DJF) and the austral winter season from June to August (JJA). During the boreal wintertime, SHF has the maximum intensity along the pathways of the western boundary currents (WBCs) and their extensions, (e.g., the Kuroshio and its extension off the coast of Japan and the Gulf Stream off the coast of North America), with magnitude exceeding 120 W m^{-2}. In the austral wintertime, SHF with moderate magnitude (<60 W m^{-2}) tends to occur in the boundary current regions in the Southern Hemisphere, such as the Agulhas Current and its extension off the coast of South Africa, the Leeuwin Current and the Eastern Australian Current off the respective western and eastern coasts of Australia, and the Brazilian/Falkland Current off the coast of South America. The intensification of SHF over the warm boundary currents reflects the continental influence on air–sea heat exchange processes. These seasonal SHF patterns are in good agreement with existing climatologies (Cayan 1992a,b; da Silva et al. 1994; Josey et al. 1998).

In addition to the boundary current regions, intense sea–air thermal exchange is observed near the sea ice edges at high latitudes. This is clearly marked by the

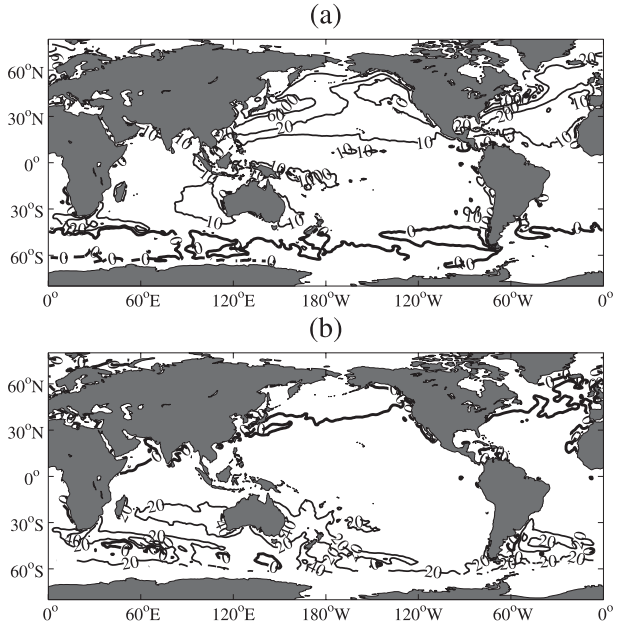

FIG. 2. Global wintertime mean SHF averaged over the 30-yr (1980–2009) period for (a) the boreal winter (DJF) and (b) the austral winter (JJA). Positive (negative) values (W m^{-2}) denote upward (downward) heat release from the ocean (atmosphere) to the atmosphere (ocean). Zero contours are highlighted by thick black lines.

narrow bands of large SHF values around the periphery of the ice zone in the Labrador Sea, the Irminger Sea, the northern Norwegian Sea, the Bering Sea, as well as in the southern oceans. Integrating along the mean ice-free edges with a 2° latitude width indicates that, on average, the magnitude of SHF is about 50 W m^{-2} along the northern edge in the boreal winter and 21 W m^{-2} along the southern edge in the austral winter (not shown). The largest SHF is found near the sea ice edges in the Norwegian Sea, with magnitude exceeding 170 W m^{-2}. It appears that the magnitude of the wintertime mean SHF near the ice edges is equivalent to that of SHF over the Gulf Stream and Kuroshio and extensions, indicative of an important role of SHF in high-latitude climate variability. Screen and Simmonds (2010) suggested that the fall/winter Arctic surface warming is likely caused by sea ice reduction due to increasing ocean heat loss (SHF + LHF). This study applied a fixed ice mask, meaning that the regions under study were ice free during the entire 30-yr period; thus the effect of shifting sea ice edges on SHF variability was not considered.

c. Decadal variability of SHF

To quantify decadal variations of SHF, the standard deviation (STD) σ of the wintertime SHF anomalies during the 30-yr period was computed for the Northern and Southern Hemispheres, respectively (Fig. 3). The STD patterns are similar to the patterns of their respective time-mean fields (Fig. 2), indicating that the regions of large absolute SHF are the regions of large year-to-year SHF variability. The zonally averaged STD (not shown) is 14.9 W m^{-2} for SHF at the northern high latitudes (north of 45°N) and 9.3 W m^{-2} for SHF at the southern high latitudes (south of 45°S). By comparison, the STD of SHF is merely 2.0 W m^{-2} at low latitudes (from 30°S to 30°N) for both seasons, which is at least 4 times smaller than the STD of SHF at high latitudes. The annual mean SHF in the tropical oceans is also weak, less than 10 W m^{-2} (Fig. 2). Obviously, SHF at high latitudes has not only larger magnitude but also larger variability than SHF at low latitudes. The sharp contrast between SHF at high and low latitudes indicates the primary modulation of high latitudes in global SHF variability.

To elucidate the high-latitude contribution to the global SHF variability, time series of monthly SHF anomalies were constructed in the following five regions (Fig. 4a): the global ice-free oceans, the northern high latitudes (north of 45°N; the northern oceans), the southern high latitudes (south of 45°S; the southern oceans), the northern + southern high latitudes, and the tropical oceans (30°S–30°N). The corresponding 30-yr monthly mean climatology was subtracted from each time series and a 5-yr running mean was applied.

The time series of global SHF shows a decadal oscillation, with a low in the mid-1980s and a high in the mid-1990s. The difference between the low and high SHF is slightly more than 1 W m^{-2}. Distinct decadal changes are also seen in the SHF time series over both the southern and northern high latitudes, albeit with different phases and amplitudes. For instance, the SHF in the southern oceans has a stronger decadal variability, marked by a low of -1.4 W m^{-2} in the mid-1980s and a high of 2.7 W m^{-2} in the mid-1990s. By comparison, the SHF variability in the northern oceans is relatively weaker, with an amplitude about half of that in the southern oceans. Additionally, the phase of the decadal variations in the northern oceans lags that in the southern oceans by about 3–5 yr. When summing up the SHF over the two high-latitude regions, the dominance of the southern oceans is clearly shown.

The tropical ocean area between 30°S and 30°N is roughly 3 times larger than the ocean regions 45° poleward and so the magnitude and variability of global SHF are dictated more by those of the tropical SHF despite that the high-latitude SHF has a much larger variability during the 30-yr period. The contribution of the high-latitude SHF is reflected more by its modulation to the

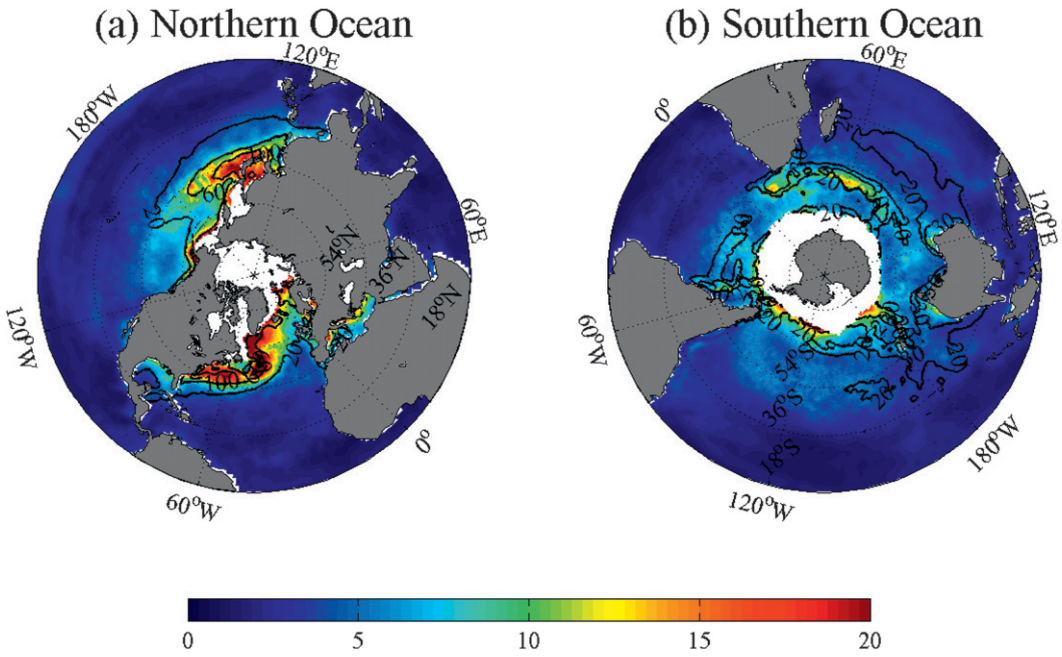

FIG. 3. Standard deviation of the wintertime mean SHF anomalies during the 30-yr (1980–2009) period for (a) the boreal winter (DJF) and (b) the austral winter (JJA). The respective 30-yr averaged winter-mean fields are superimposed [black contours; the contour interval (CI) is 40 W m^{-2} in (a) and 10 W m^{-2} in (b)].

global SHF. For instance, the global SHF from 1995 to 2000 follows the change of the high-latitude SHF rather than the tropical SHF. Moreover, the global SHF peaks in the mid-1990s, driven by the strong SHF in the southern oceans at that time. Because of the modulation, the global SHF time series does not exactly follow the tropical time series, as the latter shows a continual upward tendency until the early 2000s and has a downward tendency thereafter. It appears that tropical and high latitudes make equally important but different contributions to the decadal variability of global SHF in the past 30 yr.

The 5-yr smoothed SHF time series for the boreal winter in the northern oceans and the austral winter in the southern oceans are shown in Fig. 4b. For comparison, time series of the global SHF averaged over the two seasons (DJF and JJA) is also shown. The decadal pattern of the global SHF in the two seasons is similar to that of the global SHF constructed over all the calendar months (Fig. 4a). Therefore, the global SHF variability is modulated by the high-latitude SHF variability in the Northern and Southern Hemispheric winter seasons.

3. The thermal and wind effects on decadal SHF variability

By decomposing each variable in Eq. (1) onto the 30-yr mean (denoted by an overbar) and the yearly anomaly (denoted by a prime) relative to the mean, Eq. (1) can be rewritten as

$$Q'_{\mathrm{SHF}} \approx \rho c_p c_h [\overline{W}(\Delta T)' + W'\overline{\Delta T}] \equiv Q'_{\mathrm{therm}} + Q'_{\mathrm{wind}}, \tag{2}$$

where the term $W'(\Delta T)'$ is neglected, assuming that its contribution is much smaller than the two terms on the right-hand side of Eq. (2). This practice is commonly used by many previous studies (e.g., Cayan 1992a,b; Tanimoto et al. 2003). The thermal effect is denoted by Q'_{therm}, while the wind effect is denoted by Q'_{wind}.

To quantify the relative contributions of the thermal and wind effects to the SHF variance, the percentage of SHF anomaly Q'_{SHF} that can be explained by the two terms is calculated using the following normalized covariance, which is independent of the coefficient $\rho c_p c_h$:

$$P_{\mathrm{therm/wind}} = \frac{\mathrm{cov}(Q'_{\mathrm{therm/wind}}, Q'_{\mathrm{SHF}})}{\sqrt{\mathrm{cov}(Q'_{\mathrm{therm}}, Q'_{\mathrm{SHF}})^2 + \mathrm{cov}(Q'_{\mathrm{wind}}, Q'_{\mathrm{SHF}})^2}} \times 100\%. \tag{3}$$

Equation (3) is obtained by assuming that the terms $\overline{W}(\Delta T)'$ and $W'\overline{\Delta T}$ are not correlated so that Q'_{therm} and Q'_{wind} are independent. The contributions of the two effects are shown in Fig. 5, which depicts that the thermal

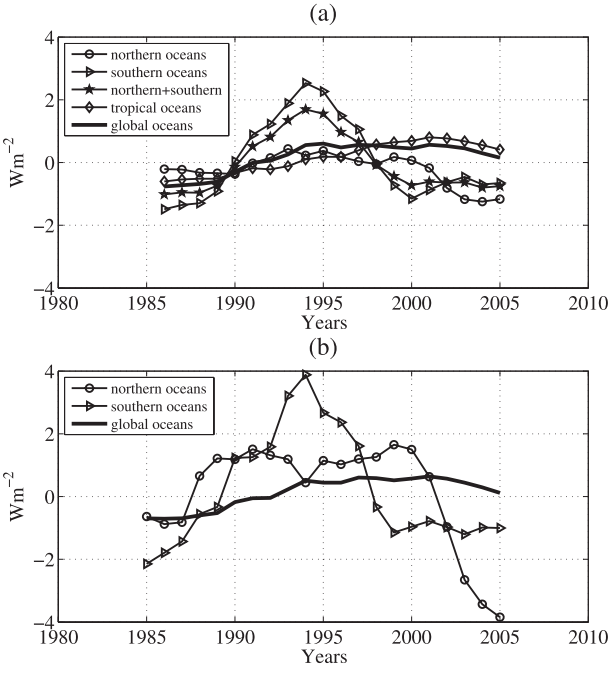

FIG. 4. (a) Time series of monthly SHF anomaly (W m^{-2}) averaged over the five regions: the global ice-free oceans, the northern oceans (poleward of 45°N), the southern oceans (poleward of 45°S), the northern plus southern oceans, and the tropical oceans (30°S–30°N). (b) Time series of the boreal winter SHF in the northern oceans, the austral winter SHF in the southern oceans, and the global SHF averaged over the boreal and the austral winter seasons. A 5-yr running mean is applied, and the beginning and end 5 yr are not plotted.

term has a predominant contribution to the year-to-year variability of the wintertime mean SHF in both hemispheres. The thermal term explains an average of 97% (99%) of the SHF yearly variances for the northern (southern) oceans, while the wind term accounts for only about 18% (7%). The total percentage explained by the thermal and wind terms is slightly more than 100% because $(a + b)/\sqrt{a^2 + b^2}$ is greater than 1 algebraically if a and b are positive. The thermal contribution is smaller (~80%) in the vicinity of the WBCs (e.g., the Kuroshio and its extension) and the Antarctic Circumpolar Current (ACC) where the changes in wind speed are large enough to partially compensate the thermal effect.

The STD of the wintertime mean sea–air temperature gradient and wind speed in the northern and southern oceans are shown in Fig. 6 with the respective mean field superimposed. The pattern of the STD of temperature gradient is similar to the pattern of the mean field, with significantly large values over the warm WBCs and their extension regions and also around the periphery of the sea ice edges. In these regions, the larger sea–air thermal difference is caused by the contrast between the relatively warm SST and the generally cold/dry SAT advected from inland. The STD of wind speed has two maxima in the northeastern Atlantic and one maximum in the eastern North Pacific. In the southern oceans, the mean structure of wind speed is basically annular, which is known as the westerly belt in the subpolar regions. Large STDs are mostly located in the southern Pacific sector.

Interestingly, the smaller thermal contribution to SHF variance in the regions of WBCs (Fig. 5) is not because the sea–air thermal contrast is small; in fact, the STD of the sea–air thermal contrast is most significant over the WBCs. The contribution by direct wind effect reflects the fact that the mean sea–air thermal gradient is already large over the WBCs during the wintertime, so that a strong perturbation in wind caused by cold air outbreak can quickly amplify the effect of the thermal background and result in significant changes in SHF. Therefore, the significance of the wind effect on SHF is dependent on the mean sea–air thermal conditions. Similarly, the significance of the thermal effect on SHF needs also to consider the mean pattern of the wind field and is not necessarily proportional to the STD of the sea–air temperature gradient.

To further elucidate the relative importance of the thermal and wind effects on SHF, time series of the wintertime mean SHF is compared with time series of the thermal and wind effect terms in the northern and southern oceans, respectively (Fig. 7). The respective 30-yr climatology mean was removed from each time series. For simplicity, the parameters such as ρ, c_p, and c_h are taken as constant, with $\rho = 1.22$ kg m^{-3}, $c_p = 1004.7$ J kg^{-1}, and $c_h = 1.5 \times 10^{-3}$ m^2 s^{-2}. The dominance of the thermal effect on the wintertime mean SHF anomalies is evident in both hemispheres, with the correlation coefficient r between the two time series being 0.8 in the northern and 0.9 in the southern oceans at the 95% confidence level. The direct contribution of the wind effect term is small, particularly so in the Southern Hemisphere.

4. Modes of SHF variability

a. The global oceans

An empirical orthogonal function (EOF) analysis was performed to the global SHF, sea–air temperature difference, and wind speed for the boreal winter (DJF) and the austral winter (JJA), respectively. Leading EOF modes for the three variables during the two seasons are shown in Fig. 8, and the associated principle components (PCs) of the leading modes are in Figs. 8g,h. The first EOF mode of global SHF variability in the boreal

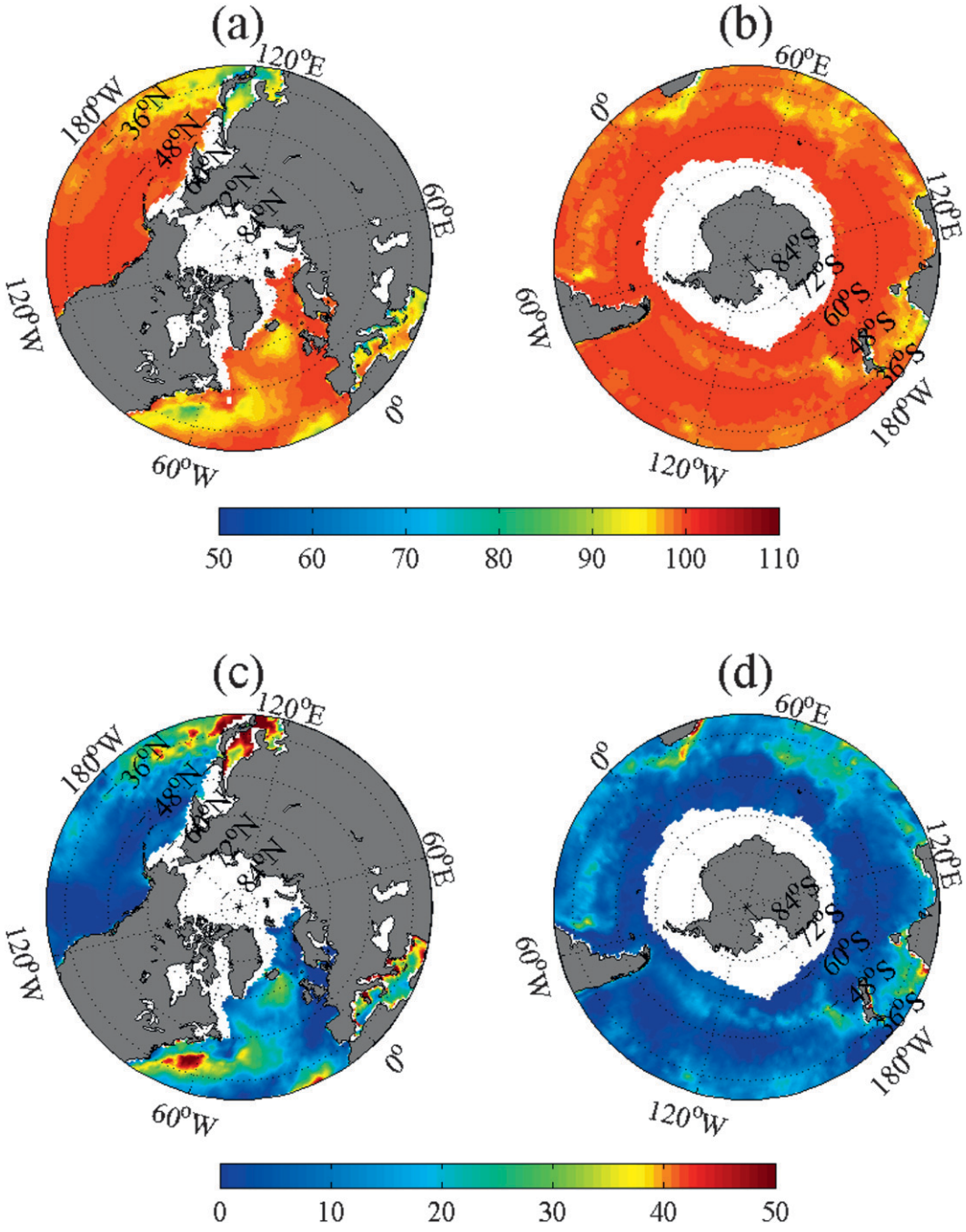

FIG. 5. Percentage of the SHF variances that is explained by the thermal effect Q'_{therm}: in (a) the northern and (b) the southern oceans and by the wind effect Q'_{wind} in (c) the northern and (d) the southern oceans. Note the change of the color scales in (c) and (d).

winter (Fig. 8a) accounts for 17.5% of the total variance and is dominated by the variability at high northern latitudes. Comparably, the first EOF mode of global SHF variability in the austral winter (Fig. 8c) accounts for the major features at high southern latitudes and explains 16.6% of the total variance. The two global EOF patterns of SHF have striking agreement with the respective leading EOF patterns of the sea–air temperature difference but differ considerably from the respective leading EOF patterns of wind speed. Again, this demonstrates the primary contribution of the thermal effect on global SHF variability.

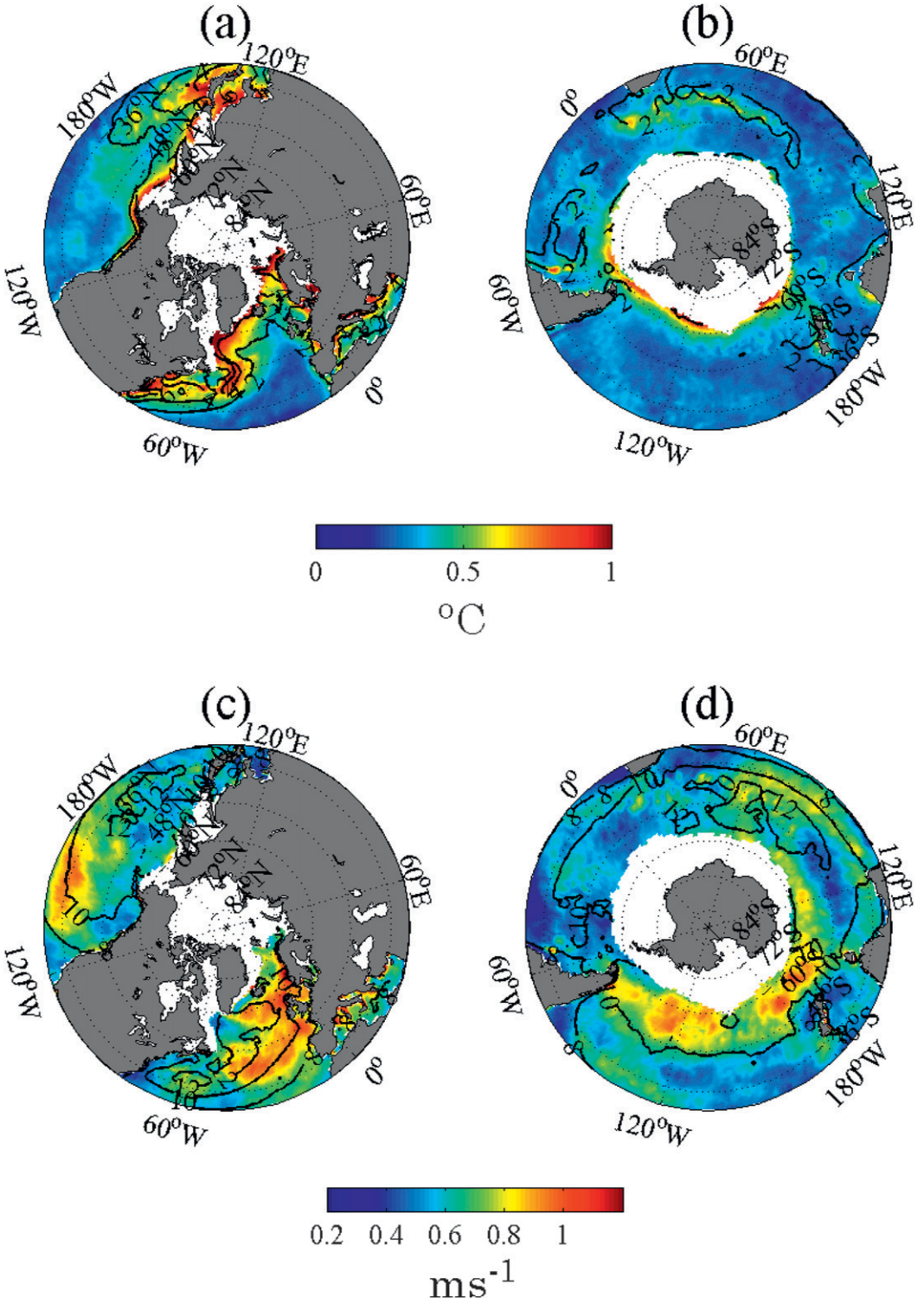

FIG. 6. STD of wintertime mean variables: (a) sea–air temperature gradient ΔT (°C) and (c) wind speed W (m s^{-1}) in the northern oceans with the respective mean field superimposed (contours). (b),(d) As in (a),(c), respectively, but for the southern oceans. The CI is 2°C in (a),(b) and 2 m s^{-1} in (c),(d).

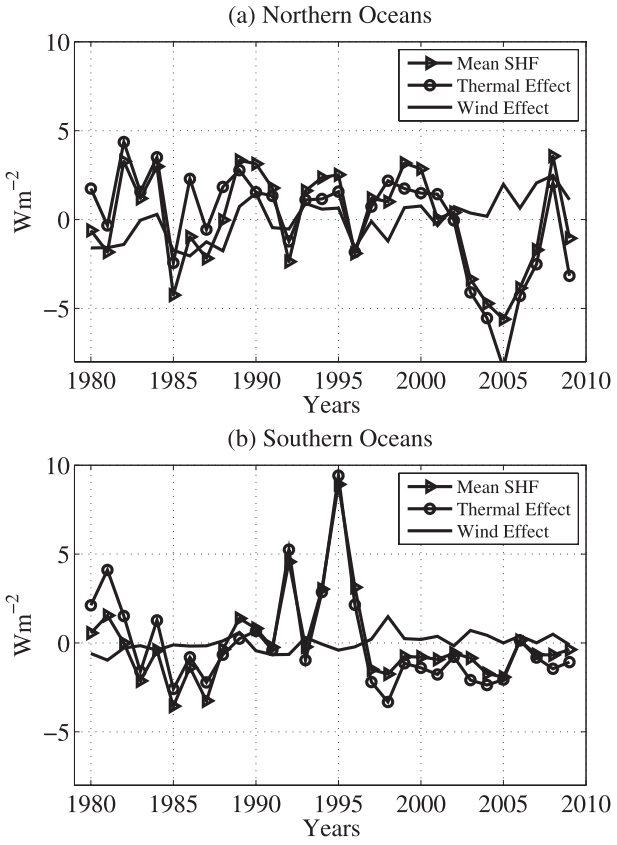

FIG. 7. Time series of wintertime mean SHF anomalies (triangles), the thermal term $\rho c_p c_h \overline{W}(\Delta T)'$, (circles), and the wind term $\rho c_p c_h W' \overline{\Delta T}$ for (a) the boreal winter in the northern oceans and (b) the austral winter in the southern oceans.

The PC associated with the first EOF mode of global wind speed in the boreal winter shows an upward trend (Figs. 8e,g) in the past three decades. A similar upward trend is also found in the austral winter (Figs. 8f,h). Nevertheless, the PC time series show again that global SHF variability in the winter seasons is governed predominantly by the thermal effect and only secondarily by the wind effect. The correlation coefficients between the PCs of SHF and the sea–air temperature difference are 0.88 and 0.78 for boreal and austral wintertime, respectively, but only 0.20 and 0.04 between SHF and wind speed for the two respective seasons.

The leading global SHF variability during the boreal winter has a pattern that strongly resembles major modes of variability in the Northern Hemisphere. In the North Pacific, the pattern of positive SHF anomalies in the east and negative SHF anomalies appears to be associated with the Pacific–North America (PNA) pattern (Wallace and Gutzler 1981). In the North Atlantic, the tripolar structure that consists of positive SHF anomalies in the subpolar region sandwiched with negative SHF anomalies in the north and south suggests an association with the North Atlantic Oscillation [(NAO), also referred to as the Arctic Oscillation (AO) or Northern Hemisphere annular mode (NAM)] (Lorenz 1950; Hurrell 1995; Thompson and Wallace 1998, 2000a). The leading global SHF mode during the austral winter features a wavelike pattern at high southern latitudes, exhibiting a connection to the Southern Hemisphere annular mode (SAM) in the form of zonal wavenumber 3 (Gong and Wang 1999; Thompson and Wallace 2000a,b; Hall and Visbeck 2002). The influence of the large-scale atmospheric circulation on SHF variability is evident. In the following two subsections, an analysis is made to understand the relationship between the leading mode of wintertime SHF variability and dominant pattern of change in basin-scale sea level pressure (SLP) and near-surface wind at northern and southern oceans.

b. The northern oceans

The leading EOF modes of the SHF and SLP in the boreal winter are shown in Figs. 9a,b, respectively, with the associated PC time series shown in Fig. 9c. The leading mode of vector wind is superimposed onto the SLP field (Fig. 9b), and a schematic diagram of the surface wind pattern is drawn on top of the SHF field. A broad agreement between the PC time series of the SHF and SLP leading modes is seen, and the correlation coefficient of the two is 0.57 and significant at a 95% confidence level.

To examine the influence of the atmospheric circulation on the SHF changes in the northern high latitude, the North Atlantic is used as a focus. SST and SAT in the North Atlantic vary with NAO. During the NAO positive phase, stronger westerly winds advect drier and colder air from the polar region, which increases the evaporation heat loss in the northern North Atlantic and further lowers SST (Cayan 1992b; Deser and Blackmon 1993). SST and SAT in the North Atlantic show similar triple structures during the positive NAO period (Fig. 10), featuring a band of cold anomalies located between 45° and 70°N sandwiched by bands of warm anomalies in its north and south. Previous studies suggest that the SST anomalies are not only driven by air–sea interactions but also modulated by ocean dynamical processes associated with the NAO (Marshall et al. 2001; Visbeck et al. 2003; Hurrell and Deser 2009). The NAO surface westerly anomalies generate variability of the North Atlantic subtropical and subpolar gyres (Curry and McCartney 2001). It is shown that mass transport of the Gulf Stream and North Atlantic Current weakens during the low NAO period, while it intensifies in the years with high NAO index, and these changes cause the changes of SST with

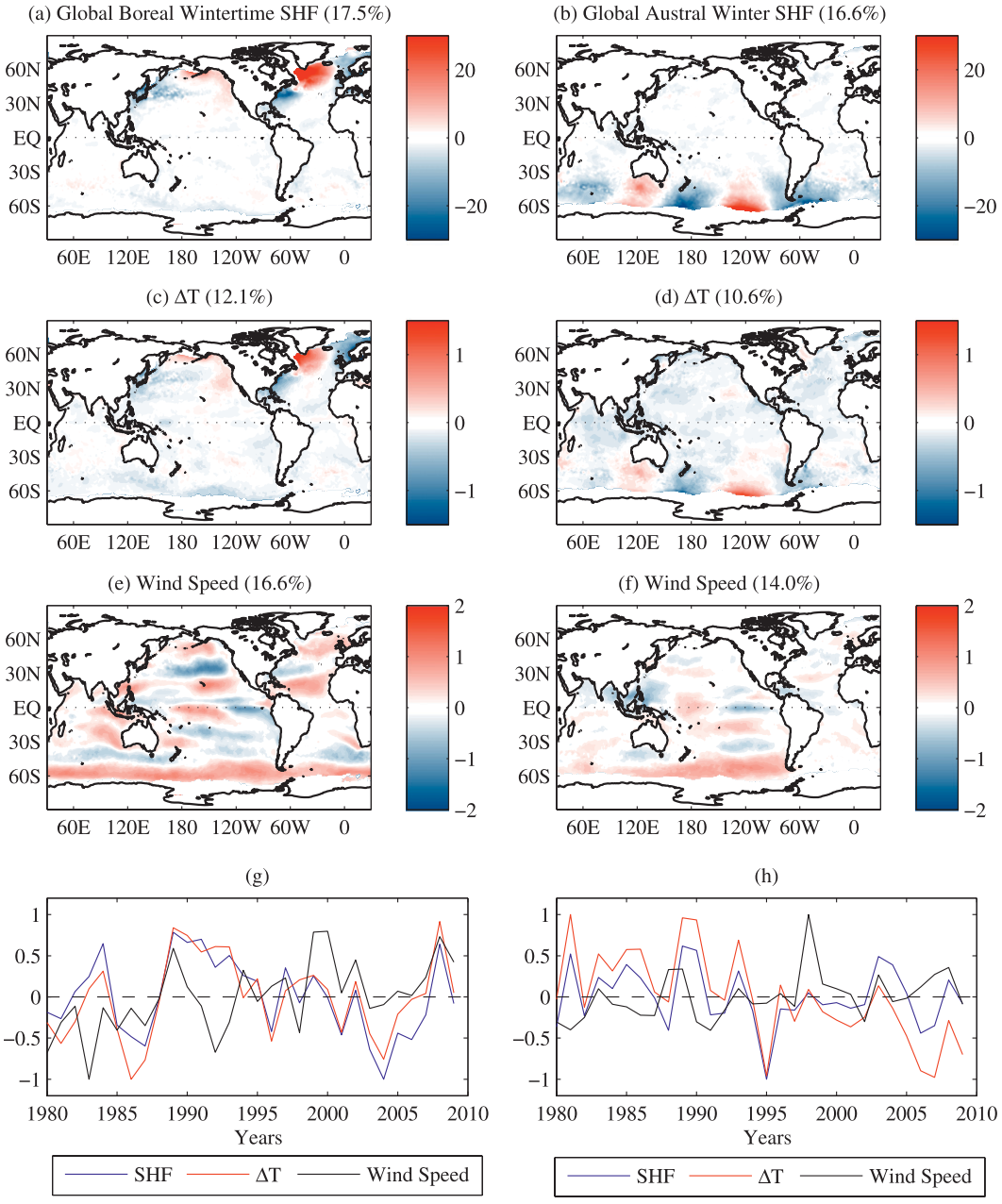

FIG. 8. (a),(b) Leading EOF modes of global SHF (W m^{-2}) in (a) the boreal winter and (b) the austral winter. (c),(d) As in (a),(b), respectively, but for the temperature gradient (°C). (e),(f) As in (a),(b), respectively, but for wind speed (m s^{-1}). (g),(h) The PCs for the leading modes in (g) the boreal winter and (h) the austral winter.

NAO phases. The magnitude of the NAO SAT anomalies is larger than that of the SST anomalies because the specific heat capacity of air is much less than the seawater, so that the SAT anomalies, or more accurately, the SAT anomalies of the reversed sign, dominate the pattern of the temperature gradient ($\Delta T = T_s - T_a$). The latter gives rise to a tripolar pattern of SHF variability on NAO time scales.

In the North Pacific sector, it seems that the change in prevailing wind associated with the prominent mode of the basin-scale circulation is also the cause of the change of SST and SAT. The leading wind pattern is associated with the negative PNA pattern (Aleutian High Anomaly), with a cyclonic surface circulation dominating the entire North Pacific. Positive anomalies of the sea–air temperature difference are seen in the north–northeastern

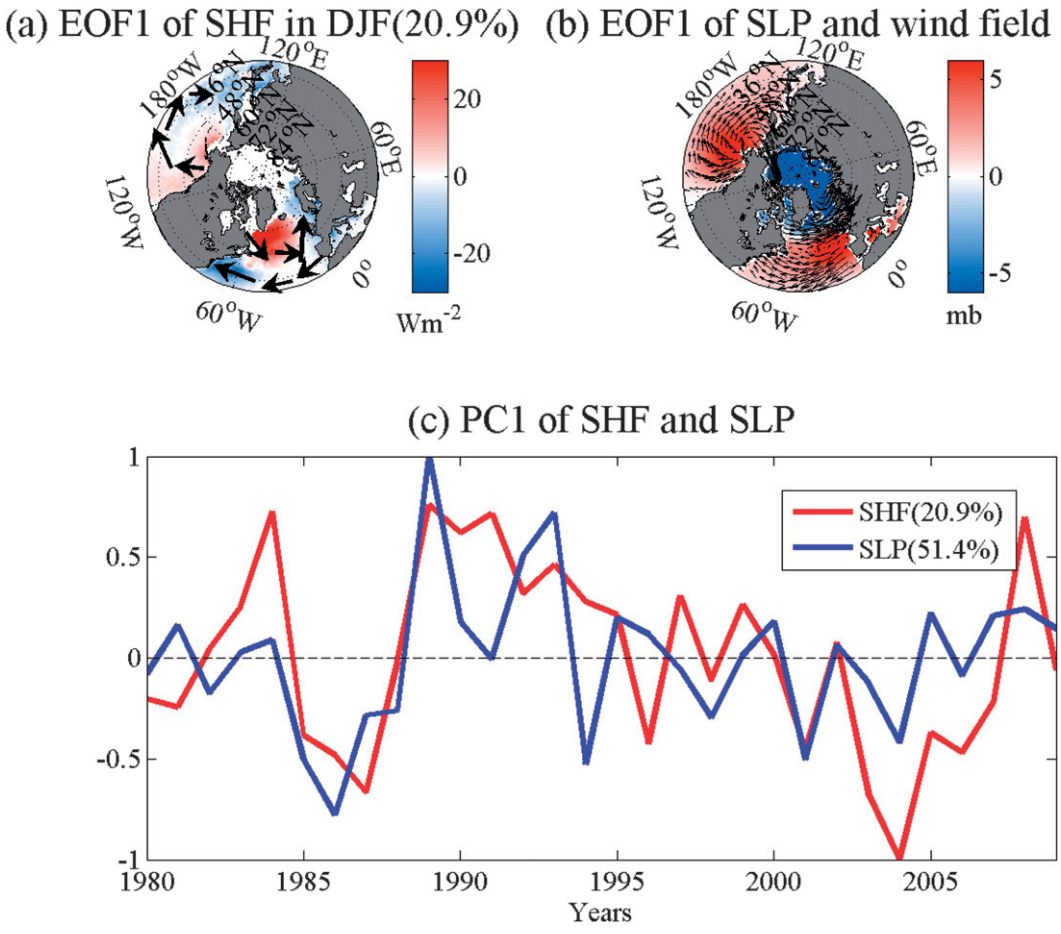

FIG. 9. Leading EOF modes of the northern oceans (a) SHF (W m^{-2}) and (b) SLP (mb) superimposed with wind vectors in the boreal winter. (c) The PCs associated with the two modes. Arrows in (a) are the schematic diagram of the wind pattern in (b).

part of the basin that is under the influence of surface northerlies from the Arctic. Conversely, the sea–air temperature difference anomalies are largely negative in regions under the direct influence of southerlies. The pattern of the sea–air temperature difference anomalies is closely related to the meridional direction of surface winds. Again, the SHF mode pattern responds to the sea–air temperature difference.

c. *The southern oceans*

The leading mode of SLP at high latitudes of Southern Hemisphere is the typical zonal symmetric SAM or Antarctic Oscillation (AAO; Gong and Wang 1999; Thompson and Wallace 2000a,b; Hall and Visbeck 2002). SAM exists in the Southern Hemisphere all year around, being most prominent in the austral winter. It has a profound influence on the Southern Hemisphere atmosphere–ocean system, inducing changes in wind, SST, SAT, the sea ice edge, the polar front, and surface heat fluxes (Thompson and Solomon 2002; Hall and Visbeck 2002; Verdy et al. 2006; Sen Gupta and England 2006, 2007; Screen et al. 2009, 2010).

Similar to the northern oceans, the leading mode of SHF in the southern oceans (Fig. 11a) can also be explained by the pattern change of SLP associated with SAM (Fig. 11b). The leading mode of vector wind is superimposed onto the SLP field (Fig. 11b), and a schematic diagram of the surface wind pattern is drawn on top of the SHF field. It can be seen that the equatorward surface winds enhance SHF, while the poleward surface winds reduce SHF. The close connection between the meridional direction of surface winds and SHF anomalies suggests again the role of the large-scale atmospheric circulation on SHF variability. The correlation coefficient between PC1 (Fig. 11c) of SHF and SLP is 0.53, similar to the correlation, 0.57, found in the northern oceans.

The annular pattern of the leading mode of SLP directly determines the zonal and meridional wind as the

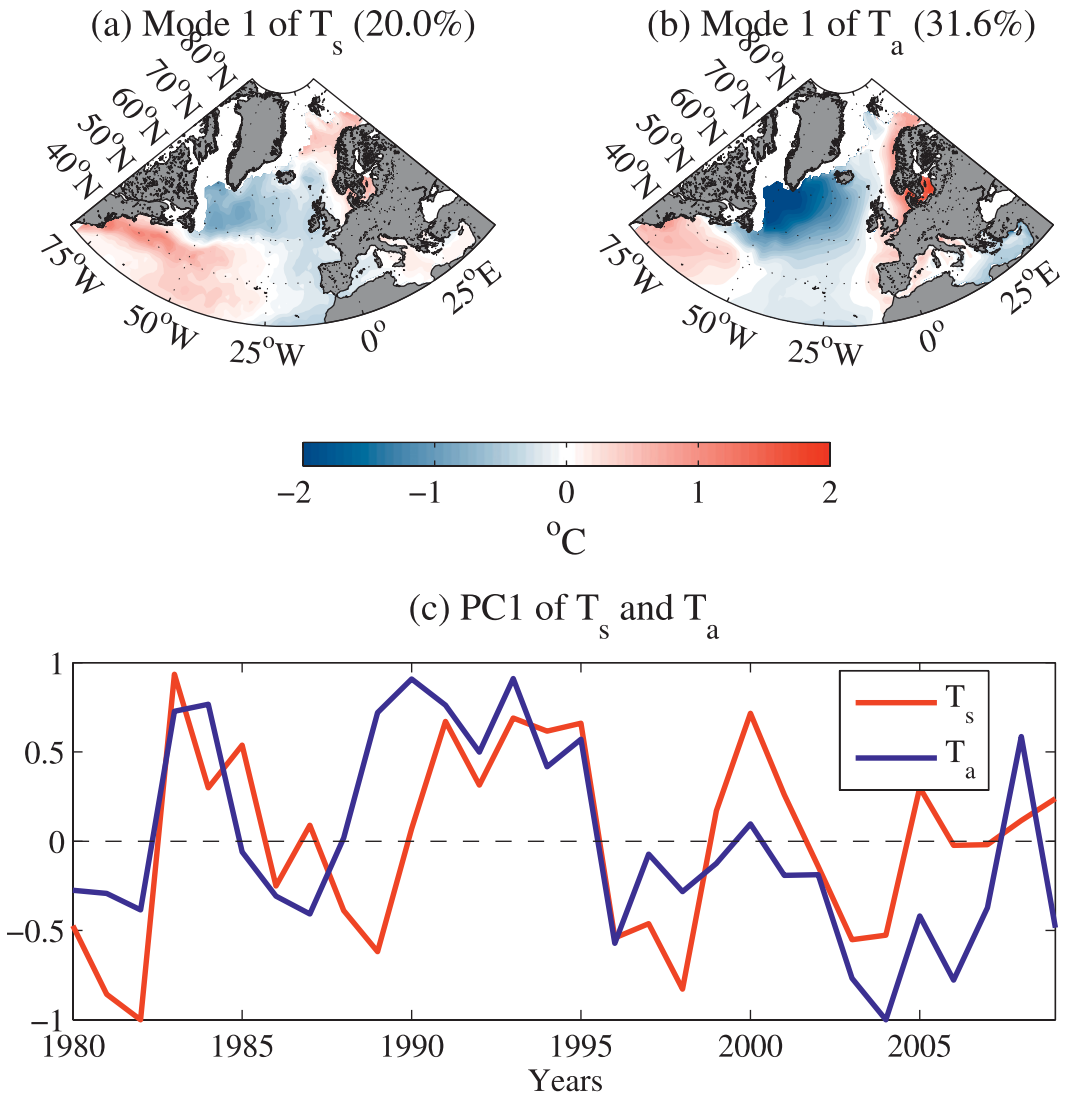

FIG. 10. The EOF1 modes of (a) SST (°C) and (b) SAT (°C) (b) in the North Atlantic sector associated with NAO. (c) The associated PC1.

large-scale wind is mostly geostrophic (Figs. 12a–f). The zonal wind EOF1 mode has a ringlike pattern similar to the SAM structure because the zonal wind is derived from the meridional pressure gradient. During the positive phase of the SAM index, it is evident that westerlies are enhanced in the subpolar regions from 50° to 70°S, while the easterly wind anomaly appears in the subtropical regions from 30° to 45°S. On the other hand, the leading mode of meridional wind shows a wavenumber-3 pattern (Fig. 12b) due to the zonal difference of the annular SLP pattern. The poleward and equatorward winds change alternately with the wave pattern.

Change of surface wind associated with SAM affects the ocean processes. The first EOF mode of SST (Fig. 12c) also shows a ringlike zonal symmetric pattern, with a band of cold SST near the edge of the Antarctic continent and the southern Atlantic sector, which is consistent with the enhanced westerly in these regions. The Ekman drift due to zonal wind is suggested to be a mechanism that governs SST variability on the SAM time scale (Hall and Visbeck 2002; Oke and England 2004; Sen Gupta and England 2006; Böning et al. 2008; Ito et al. 2010; Sallée et al. 2010). The Ekman drift can cause polar cold water to move equatorward and induce a cold water band on the edge of the Antarctic Continent. Meanwhile, the southward eddy fluxes compensate the northward Ekman transport, resulting in warmer SST in the southern oceans. It is found that the eddy flux compensation is also a cause of the warmer

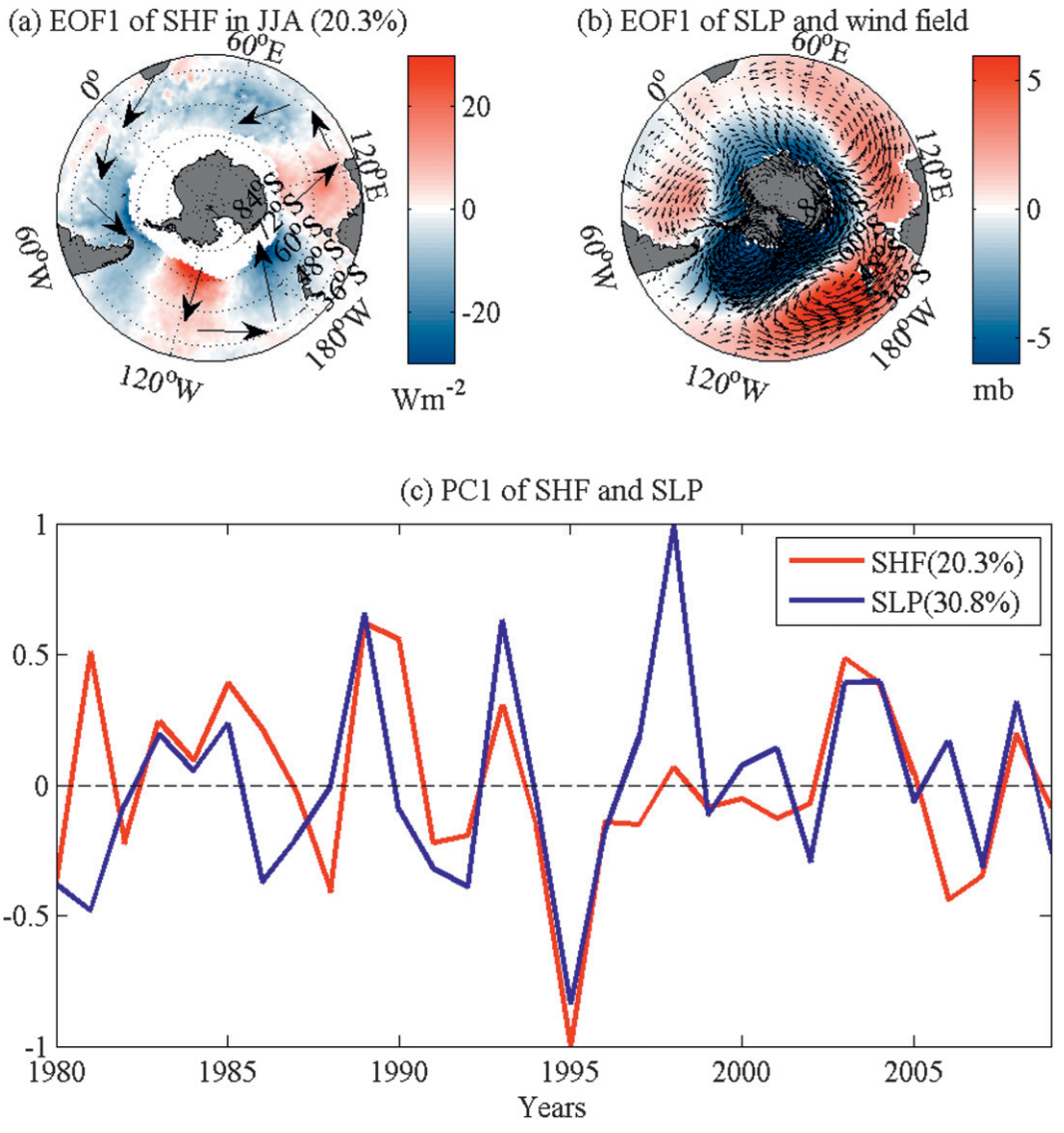

FIG. 11. As in Fig. 9, but for the austral winter in the southern oceans.

SST in the western boundary currents regions of the Southern Hemisphere, such as the Brazil–Malvinas Current confluence and the East Australian Current separation (Fig. 12c) (Meredith and Hogg 2006; Hogg et al. 2008; Screen et al. 2009).

The leading SAT mode (Fig. 12d) has also a wavenumber-3 pattern, which is caused by the southerly (northerly) winds that advect cooler (warmer) air to the north (south) and produce regionally lower (higher) SAT (Karpechko et al. 2009). Similar to the findings from the analysis of the northern oceans, the SAT anomalies of reserves sign are the driver of the anomalies of the sea–air temperature difference, which give rise to the pattern of SHF variability.

5. Summary

The study examined global variability of air–sea sensible heat flux during the 30-yr period from 1980 to 2009 and the large-scale atmospheric and ocean circulations that gave rise to this variability. The contribution of high-latitude wintertime SHF was identified and the effects of the sea–air temperature difference wind speed on decadal change of SHF were analyzed.

An empirical orthogonal function (EOF) analysis was performed for SHF in three cases: the high northern latitudes during the boreal winter, the high southern latitudes during the austral winter, and the global basin during the calendar year. The results show that global

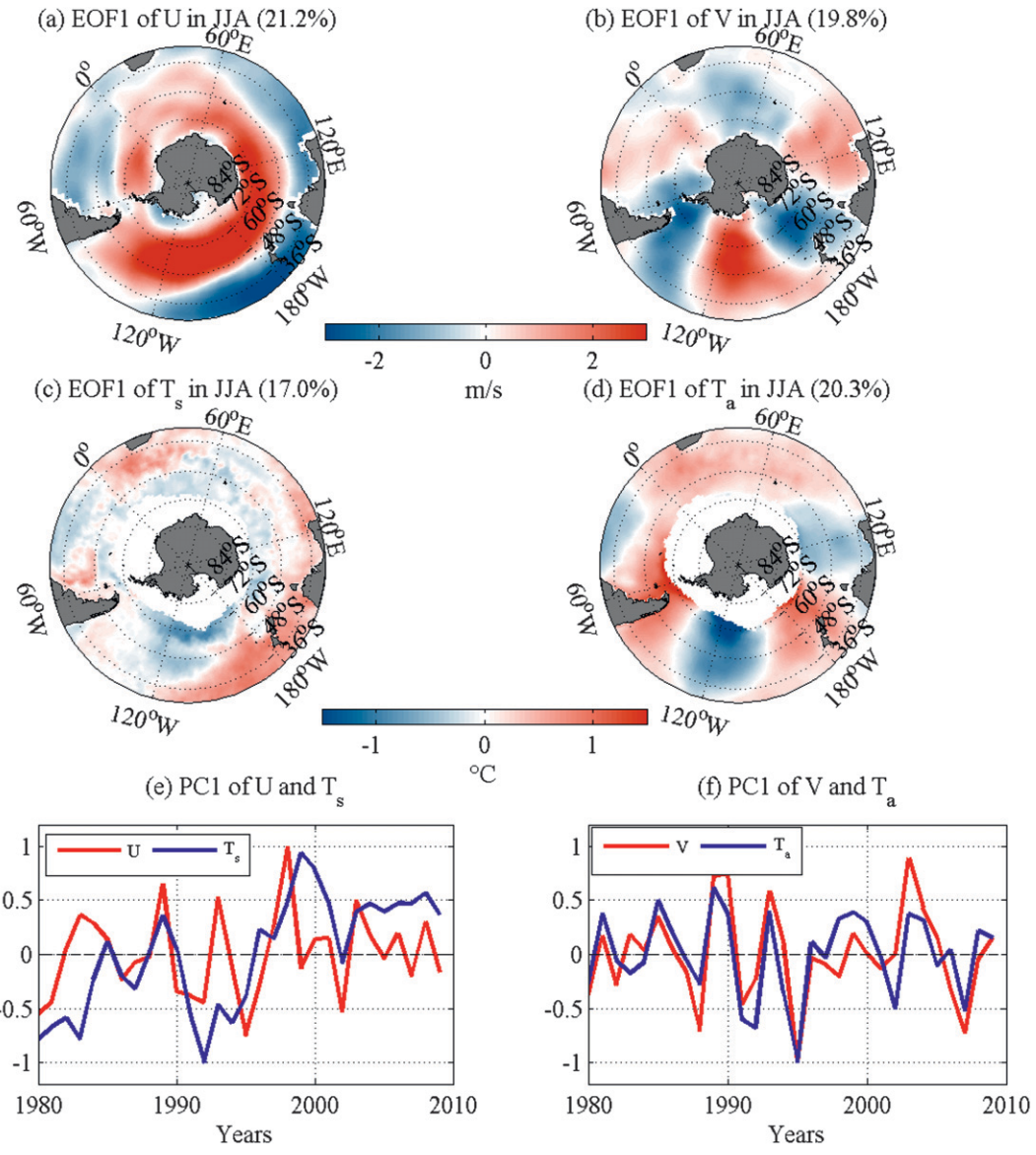

FIG. 12. Leading EOF modes of (a) zonal wind U (m s^{-1}), (b) meridional wind V (m s^{-1}), (c) SST (T_s, °C), and (d) SAT (T_a, °C) in the southern oceans during the austral winter. (e),(f) The PC1 of (e) U and SST and (f) V and SAT.

SHF anomalies are strongly modulated by SHF at high latitudes (poleward of 45°) during winter seasons. To summarize this result, yearly time series of global SHF in the two seasons, the boreal winter (DJF) and the austral winter (JJA), is compared with the sum of the two EOF1 modes, namely, the boreal wintertime SHF in the northern oceans and the austral wintertime SHF (JJA) in the southern oceans (Fig. 13). Apparently, decadal variability of global SHF in the two seasons can be reasonably represented by the two leading high-latitude SHF modes in their respective winter seasons. Differences do exist. For instance, the time series of global SHF and the high-latitude SHF both trended upward before 2000, albeit the former tended to lag the latter by about one year during much of the period. Since 2000, the global wintertime mean has trended downward steadily, while the high-latitude modes tended to be more variable with a major drop in 2003/04. It appears that the increase of global SHF in the mid-1990s is attributable to the strengthening of the SAM index during this period (Figs. 4b and 11c), while the decrease of global SHF thereafter is due primarily to the downward trend of the AO index (Figs. 4b and 9c). Evidently, global wintertime SHF is modulated by the prominent modes of the large-scale atmospheric

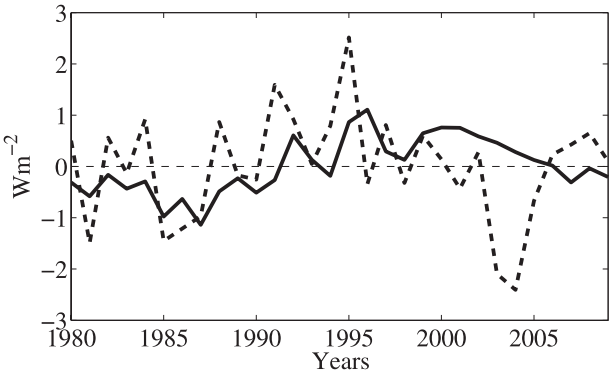

FIG. 13. Global SHF variability (solid) averaged over the boreal winter (DJF) and the austral winter (JJA) vs the sum of the two leading modes (dashed): the boreal winter SHF in the northern oceans and the austral winter SHF in the southern oceans.

circulation at high latitudes, namely, the NAO and PNA in the Northern Hemisphere and the SAM in the Southern Hemisphere.

The wintertime SHF variability is governed primarily by the sea–air temperature difference (i.e., the thermal effect) and only slightly by direct wind speed. However, this does not mean that wind is not important. In fact, one major finding of the study is that the direction of surface wind has played a critical role in modulating the sea–air temperature gradient by advecting cold and dry air from continents to the relatively warmer water surface and by imposing changes in wind-driven oceanic processes that affect SST. It is found that the pattern of air temperature anomalies dominates over the pattern of SST anomalies and dictates the pattern of decadal SHF variability.

This study identified the important effects of wind direction and speed on SHF variability. This finding is in tune with the study of Yu (2007) that shows the important role of winds in enhancing global evaporation in the past 50 yr. Taken together, winds are a critical player in the observed global variability of air–sea turbulent latent and sensible heat exchange.

Acknowledgments. The study is supported by the NOAA Office of Climate Observations (OCO) and the WHOI Arctic Climate Initiative. X. Song acknowledges the support from the China Scholarship Council, National Natural Science Foundation of China (NSFC) (40930844, 40976004, and 40921004) and the Ministry of Education's 111 Project (B07036). The WHOI Academic Programs Office is acknowledged for hosting X. Song as a visiting student for two years. We thank X. Jin for providing monthly OAFlux datasets for the study, and Shirley Cabral McDonald for editorial assistance with this manuscript. Two anonymous reviewers are acknowledged for their constructive and valuable comments. OAFlux datasets are available from the project website http://oaflux.whoi.edu/. NCEP–DOE 2 reanalysis data are provided by NOAA/OAR/ESRL PSD, Boulder, Colorado, from their website at http://www.esrl.noaa.gov/psd/.

REFERENCES

Allen, M. R., and W. J. Ingram, 2002: Constraints on future changes in climate and the hydrologic cycle. *Nature,* **419,** 224–232.

Andersson, A., S. Bakan, K. Fennig, H. Grassl, C.-P. Klepp, and J. Schulz, 2007: Hamburg ocean atmosphere parameters and fluxes from satellite data—HOAPS-3 monthly mean. World Data Center for Climate Rep., doi:10.1594/WDCC/HOAPS3_MONTHLY.

Bala, G., P. B. Duffy, and K. E. Taylor, 2008: Impact of geoengineering schemes on the global hydrological cycle. *Proc. Natl. Acad. Sci. USA,* **105,** 7664–7669.

Berry, D. I., and E. C. Kent, 2009: A new air–sea interaction gridded dataset from ICOADS with uncertainty estimates. *Bull. Amer. Meteor. Soc.,* **90,** 645–656.

——, and ——, 2011: Air-sea fluxes from ICOADS: The construction of a new gridded dataset with uncertainty estimates. *Int. J. Climatol.,* **11,** 987–1001, doi:10.1002/joc.2059.

Boer, G. J., 1993: Climate change and the regulation of the surface moisture and energy budgets. *Climate Dyn.,* **8,** 225–239.

Böning, C. W., A. Dispert, M. Visbeck, S. R. Rintoul, and F. U. Schwarzkopf, 2008: The response of the Antarctic Circumpolar Current to recent climate change. *Nat. Geosci.,* **1,** 864–869.

Carton, J. A., and Z. Zhou, 1997: Annual cycle of sea surface temperature in the tropical Atlantic Ocean. *J. Geophys. Res.,* **102** (C13), 27 813–27 824.

Cayan, D. R., 1992a: Latent and sensible flux over the north oceans: The connection to monthly atmosphere circulation. *J. Climate,* **5,** 354–369.

——, 1992b: Latent and sensible flux over the north oceans: Driving the sea surface temperature. *J. Phys. Oceanogr.,* **22,** 859–881.

Curry, R. D., and M. S. McCartney, 2001: Ocean gyre circulation changes associated with the North Atlantic Oscillation. *J. Phys. Oceanogr.,* **31,** 3374–3400.

da Silva, A., C. C. Young, and S. Levitus, 1994: *Atlas of Surface Marine Data 1994*. Vol. 1, *Algorithms and Procedures,* NOAA Atlas NESDIS 6, 83 pp.

Deser, C., and M. L. Blackmon, 1993: Surface climate variations over the North Atlantic Ocean during winter. *J. Climate,* **6,** 1743–1753.

Fairall, C. W., E. F. Bradley, J. E. Hare, A. A. Grachev, and J. B. Edson, 2003: Bulk parameterization on air–sea fluxes: Updates and verification for the COARE algorithm. *J. Climate,* **16,** 571–591.

Foltz, G. R., and M. J. McPhaden, 2005: Mixed layer heat balance on intraseasonal time scales in the northwestern tropical Atlantic Ocean. *J. Climate,* **18,** 4168–4184.

——, J. Vialard, B. P. Kumar, and M. J. McPhaden, 2010: Seasonal mixed layer heat balance of the southwestern tropical Indian Ocean. *J. Climate,* **23,** 947–965.

Gleckler, P. J., and B. C. Weare, 1997: Uncertainties in global ocean surface heat flux climatologies derived from ship observations. *J. Climate,* **10,** 2764–2781.

Gong, D., and S. Wang, 1999: Definition of Antarctic Oscillation index. *Geophys. Res. Lett.,* **26,** 459–462.

Grossman, R. L., and A. K. Betts, 1990: Air–sea interaction during an extreme cold air outbreak from the eastern coast of United States. *Mon. Wea. Rev.,* **118,** 324–342.

Hall, A., and M. Visbeck, 2002: Synchronous variability in the Southern Hemisphere atmosphere, sea ice, and ocean resulting from the annular mode. *J. Climate,* **15,** 3043–3057.

Held, I. M., and B. J. Soden, 2006: Robust responses of the hydrological cycle to global warming. *J. Climate,* **19,** 5686–5699.

Hogg, A. M., M. P. Meredith, J. R. Blundell, and C. Wilson, 2008: Eddy heat flux in the Southern Ocean: Response to variable wind forcing. *J. Climate,* **21,** 608–620.

Hurrell, J. W., 1995: Decadal trends in the North Atlantic Oscillation: Regional temperatures and precipitation. *Science,* **269,** 676–679.

——, and W. C. Deser, 2009: North Atlantic climate variability: The role of the North Atlantic Oscillation. *J. Mar. Syst.,* **79,** 231–244.

Ito, T., M. Woloszyn, and M. Mazloff, 2010: Anthropogenic carbon dioxide transport in the Southern Ocean driven by Ekman flow. *Nature,* **463,** 80–84.

Josey, S. A., E. C. Kent, and P. K. Taylor, 1998: The Southampton Oceanography Centre (SOC) ocean–atmosphere heat, momentum and freshwater flux atlas. Southampton Oceanography Centre Rep. 6, 30 pp.

Kanamitsu, M., and Coauthors, 2002: NCEP-DOE AMIP-II Reanalysis (R-2). *Bull. Amer. Meteor. Soc.,* **83,** 1631–1643.

Karpechko, A. Y., N. P. Gillett, G. J. Marshall, and J. A. Screen, 2009: Climate impacts of the Southern Annular Mode simulated by the CMIP3 models. *J. Climate,* **22,** 3751–3768.

Kiehl, J. T., and K. E. Trenberth, 1997: Earth's annual global mean energy budget. *Bull. Amer. Meteor. Soc.,* **78,** 197–208.

Kubota, K., A. Kano, H. Muramatsu, and H. Tomita, 2003: Intercomparison of various surface latent heat flux fields. *J. Climate,* **16,** 670–678.

Kubota, M., N. Iwasaka, S. Kizu, M. Konda, and K. Kutsuwada, 2002: Japanese ocean flux datasets with use of remote sensing observations (J-OFURO). *J. Oceanogr.,* **58,** 213–225.

Liu, J., T. Xiao, and L. Chen, 2010: Intercomparisons of air-sea heat flux over the Southern Ocean. *J. Climate,* **24,** 1198–1211.

Liu, W. T., K. B. Katsaros, and J. A. Businger, 1979: Bulk parameterization of air–sea exchanges of heat and water vapor including the molecular constraints at the interface. *J. Atmos. Sci.,* **36,** 1722–1735.

Lorenz, E. N., 1950: Seasonal and irregular variations of the Northern Hemisphere sea-level pressure profile. *J. Meteor.,* **8,** 52–59.

Marshall, J., and Coauthors, 2001: North Atlantic climate variability, phenomena, impacts and mechanisms. *Int. J. Climatol.,* **21,** 1863–1898.

Meredith, M. P., and A. M. Hogg, 2006: Circumpolar response of Southern Ocean eddy activity to a change in the Southern Annular Mode. *Geophys. Res. Lett.,* **33,** L16608, doi:10.1029/2006GL026499.

Nigam, S., and Y. Chao, 1996: Evolution dynamics of tropical ocean–atmosphere annual cycle variability. *J. Climate,* **9,** 3187–3205.

Oke, P. R., and M. H. England, 2004: Oceanic response to changes in the latitude of the Southern Hemisphere subpolar westerly winds. *J. Climate,* **17,** 1040–1054.

Pagowski, M., and G. W. K. Moore, 2001: A numerical study of an extreme cold-air outbreak over the Labrador Sea: Sea ice, air–sea interaction, and development of polar lows. *Mon. Wea. Rev.,* **129,** 47–72.

Renfrew, I. A., and G. W. K. Moore, 1999: An extreme cold-air outbreak over the Labrador Sea: Roll vortices and air–sea interaction. *Mon. Wea. Rev.,* **127,** 2379–2394.

——, ——, P. S. Guest, and K. Bumke, 2002: A comparison of surface boundary layer and surface turbulence heat flux observations over the Labrador Sea with ECMWF analyses and NCEP reanalyses. *J. Phys. Oceanogr.,* **32,** 383–400.

Sallée, J. B., K. G. Speer, and S. R. Rintoul, 2010: Zonally asymmetric response of the Southern Ocean mixed-layer depth to the Southern Annular Mode. *Nat. Geosci.,* **3,** 273–279.

Screen, J., and I. Simmonds, 2010: Increasing fall-winter energy loss from the Arctic Ocean and its role in Arctic temperature amplification. *Geophys. Res. Lett.,* **37,** L16707, doi:10.1029/2010GL044136.

——, N. Gillett, D. Stevens, G. Marshall, and H. Roscoe, 2009: The role of eddies in the Southern Ocean temperature response to the Southern Annular Mode. *J. Climate,* **22,** 806–818.

——, ——, and A. Karpechko, 2010: Mixed layer temperature response to the Southern Annular Mode: Mechanisms and model representation. *J. Climate,* **23,** 664–678.

Sen Gupta, A., and M. H. England, 2006: Coupled ocean–atmosphere–ice response to variations in the Southern Annular Mode. *J. Climate,* **19,** 4457–4486.

——, and ——, 2007: Coupled ocean–atmosphere feedback in the Southern Annular Mode. *J. Climate,* **20,** 3677–3692.

Smith, S. R., P. J. Hughes, and M. A. Bourassa, 2011: A comparison of nine monthly air-sea flux products. *Int. J. Climatol.,* **31,** 1002–1027, doi:10.1002/joc.2225.

Tanimoto, Y., H. Nakamura, T. Kagimoto, and S. Yamane, 2003: An active role of extratropical sea surface temperature anomalies in determining anomalous turbulent heat flux. *J. Geophys. Res.,* **108,** 3304, doi:10.1029/2002JC001750.

Thompson, D. W. J., and J. M. Wallace, 1998: The Arctic Oscillation signature in the winter time geopotential height and temperature fields. *Geophys. Res. Lett.,* **25,** 1297–1300.

——, and ——, 2000a: Annular modes in the extratropical circulation. Part I: Month-to-month variability. *J. Climate,* **13,** 1000–1016.

——, and ——, 2000b: Annular modes in the extratropical circulation. Part II: Trends. *J. Climate,* **13,** 1018–1036.

——, and S. Solomon, 2002: Interpretation of recent Southern Hemisphere climate change. *Science,* **296,** 895–899.

Trenberth, K. E., J. T. Fasullo, and J. Kiehl, 2009: Earth's global energy budget. *Bull. Amer. Meteor. Soc.,* **90,** 311–323.

Våge, K., and Coauthors, 2009: Surprising return of deep convection to the subpolar North Atlantic Ocean in winter 2007–2008. *Nat. Geosci.,* **2,** 67–72.

Verdy, A., J. Marshall, and A. Czaja, 2006: Sea surface temperature variability along the path of the Antarctic Circumpolar Current. *J. Phys. Oceanogr.,* **36,** 1317–1331.

Visbeck, M., E. P. Chassignet, R. G. Curry, T. L. Delworth, R. R. Dickson, and G. Krahmann, 2003: The ocean's response to North Atlantic Oscillation variability. *The North Atlantic Oscillation: Climatic Significance and Environmental Impact, Geophys. Monogr.,* Vol. 134, Amer. Geophys. Union, 113–146.

Wallace, J. M., and D. S. Gutzler, 1981: Teleconnections in the geopotential height field during the Northern Hemisphere winter. *Mon. Wea. Rev.,* **109,** 784–812.

——, C. Smith, and C. S. Bretherton, 2007: Singular-value decomposition of wintertime sea surface temperature and 500-mb height anomalies. *J. Climate,* **5,** 541–560.

Wentz, F. J., L. Ricciardulli, K. Hilburn, and C. Mears, 2007: How much more rain will global warming bring? *Science,* **317,** 233–235.

Xue, H., J. M. Bane, and L. M. Goodman, 1995: Modification of the Gulf Stream through strong air–sea interactions in winter: Observations and numerical simulations. *J. Phys. Oceanogr.,* **25,** 533–557.

Yu, L., 2007: Global variations in oceanic evaporation (1958–2005): The role of the changing wind speed. *J. Climate,* **20,** 5376–5390.

——, and R. A. Weller, 2007: Objectively analyzed air–sea heat fluxes for the global ice-free oceans (1981–2005). *Bull. Amer. Meteor. Soc.,* **88,** 527–539.

——, and ——, 2009: Global ocean heat fluxes. *Bull. Amer. Meteor. Soc.,* **90,** S1–S196.

——, X. Jin, and R. A. Weller, 2008: Multidecade global flux datasets from the Objectively Analyzed Air-sea Fluxes (OAFlux) Project: Latent and sensible heat fluxes, ocean evaporation, and related surface meteorological variables. Woods Hole Oceanographic Institution OAFlux Project Tech. Rep. OA-2008-01, 64 pp.